Potential for larger earthquakes in the East San Francisco Bay Area due to the direct connection between the Hayward and Calaveras Faults

E. Chaussard [1,2], R. Bürgmann [1,2], H. Fattahi [3], R. M. Nadeau [1,2], T. Taira[1,2], C.W. Johnson [1,2], and I. Johanson [1,2]

(1) Department of Earth and Planetary Science, University of California, Berkeley, Berkeley, California

(2) Berkeley Seismological Laboratory, University of California, Berkeley, California

(3) Rosenstiel School of Marine and Atmospheric Science, University of Miami, Miami, FL

Corresponding author: Estelle Chaussard, 382 McCone Hall University of California Berkeley, Berkeley CA 94720-4767, USA (estelle@seismo.berkeley.edu)

This article has been accepted for publication and undergone full peer review but has not been through the copyediting, typesetting, pagination and proofreading process which may lead to differences between this version and the Version of Record. Please cite this article as doi: 10.1002/2015GL063575

Abstract

The Hayward and Calaveras Faults, two strike-slip faults of the San Andreas System located in the East San Francisco Bay Area, are commonly considered independent structures for seismic hazard assessment. We use InSAR to show that surface creep on the Hayward Fault continues 15 km farther south than previously known, revealing new potential for rupture and damage south of Fremont. The extended trace of the Hayward Fault, also illuminated by shallow repeating micro-earthquakes, documents a surface connection with the Calaveras Fault. At depths greater than 3-5 km, repeating micro-earthquakes located 10 km north of the surface connection highlight the 3-D wedge geometry of the junction. Our new model of the Hayward and Calaveras Faults argues that they should be treated as a single system with potential for earthquake ruptures generating events with magnitudes greater than 7, posing a higher seismic hazard to the East San Francisco Bay Area than previously considered.

Highlights

- Active faults' structure can be illuminated using space geodesy and seismology
- Hayward and Calaveras Faults are directly connected on surface and at depth
- Earthquakes of M>7 could occur on the Hayward-Calaveras Fault system.

Keywords

Hayward-Calaveras Faults; InSAR; Characteristically Repeating Earthquakes; Connection; Creep

1. Introduction

Fault geometry and connectivity directly influence seismic hazard, as an earthquake‘s magnitude greatly depends on the rupture area. Step-overs and other complex fault connections have controlled rupture lengths of many earthquakes and are considered to act as barriers to rupture propagation, limiting maximum earthquake magnitudes [*Wesnousky*, 2008; *Lozos et al.*, 2014]. Such a step-over has been documented between the Calaveras and Hayward Faults (CF and HF, respectively) [*Aydin and Page*, 1984], major components of the San Andreas Fault System in the East San Francisco Bay Area that accommodate ~15 mm/yr (~30%) of the relative motion between the North American and Pacific plates [*Field et al., 2015*]. Interseismic deformation on the CF and HF comprises both stress accumulation on locked sections of the faults and steady-state or episodic aseismic slip [*Lienkaemper et al.*, 2014]. Because creep rates are lower than long-term slip rates, these two faults are capable of producing large earthquakes, as shown by the occurrence of six M=5.5-7 events since 1850 with rupture lengths up to tens of kilometers [*Oppenheimer et al.*, 2010]. The HF is the most hazardous fault in the Bay Area given that a full average recurrence interval has passed since its last M~7 earthquake in 1868 [*Field et al., 2015*]. From the limited historical records no rupture encompassed both the HF and CF and paleoseismic trenching studies, which estimate recurrence times by considering older earthquakes [*Lienkaemper et al.*, 2010; *Simpson et al.*, 1999], are not able to assess the extent of events. Accordingly, the potential for large, cascading multi-segment ruptures cannot be ruled out, especially if the CF and HF are connected.

Over the years, many maps have shown surface traces of the HF and CF that do not intersect [*Simpson et al.*, 1999; *Graymer et al.*, 2007] (Figure 1). The northern

segment of the CF (north CF) trends subparallel to the HF for a distance of ~60 km and transitions into the central CF segment near 37°24'N where a change in strike from ~N25°W to ~N32°W occurs (Figure 1). Evidence based on relocated micro-earthquakes, seismic reflection studies, geologic mapping, gravity and magnetic data have argued for a connection between the CF and HF at depths greater than 5 km below Mission Peak [*Andrews et al.,* 1998; *Ponce et al.,* 2004; *Manaker et al.,* 2005; *Williams et al.,* 2005; *Graymer et al.,* 2007; *Hardebeck, et al.,* 2007]. However, this deep through-going structure is believed to be associated with a complex network of faults at shallower depths, challenging the consideration of the CF-HF junction in hazard models and ground motion simulations. The most recent models and simulations have recognized the importance of multi-fault ruptures [*Aagaard et al.,* 2010; *Field et al., 2015*] but the ambiguous location of the active surface trace of the HF south of the city of Fremont remains the most limiting factor in fully characterizing the structure of the CF-HF junction.

The traditionally mapped CF and HF surface traces are based on spatially limited field observations that may be misinterpreted due to the existence of multiple active and inactive fault strands and on LiDAR (Light Detection And Ranging), which enables mapping with a high spatial resolution but remains uncertain due to the scarcity of large offsets and the abundance of landslides [*U.S. Geological Survey and California Geological Survey,* 2015; *Mynatt et al.,* 2008]. InSAR (Interferometric Synthetic Aperture Radar) observations of surface creep have been used to identify the HF trace in urban areas [*Schmidt et al.,* 2005; *Shirzaei and Bürgmann,* 2013], but the fault trace has not been successfully delineated in vegetated hillsides due to loss of coherence (temporal difference in reflection of the radio waves). To overcome this limitation we use a large dataset of SAR images and modify the small baseline subset

(SBAS) time series method [*Berardino et al.,* 2002] to select only interferograms with optimal coherence.

2. Methods

2.1. InSAR method

We resolve the 1992-2011 interseismic deformation in the San Francisco Bay Area using InSAR time-series analysis of ERS and Envisat data, with > 250 acquisitions from 4 tracks (2 descending: 70 and 299, and 2 ascending: 206 and 478) and 6 frames (2853, 729, 747) provided through the WInSAR archive. We use the Modular SAR Processor software from Gamma Remote Sensing to generate Single Look Complex data and the ROI_PAC software [*Rosen et al.,* 2004] to produce over 1200 interferograms. We remove topographic contributions using the 1-arc second Shuttle Radar Topography Mission (SRTM) digital elevation model [*Farr and Kobrick,* 2000]. We co-register the wrapped interferograms of each frame to a master image, use the statistical-cost network-flow algorithm for phase unwrapping (SNAPHU; [*Chen and Zebker,* 2001]), and reference all interferograms to a pixel collocated with the GPS station LUTZ.

We invert for the phase history at each epoch relative to the first using a least square approach (SBAS) applied to fully connected networks of interferograms so that the design matrices have full ranks [*Berardino et al.,* 2002]. To maintain coherence in vegetated areas, we develop an alternative interferogram selection that directly accounts for the level of spatial coherence in each interferogram. Only interferograms with a high percentage of pixels (50%) above a sufficient spatial correlation (0.5) in our area of interest that comprises vegetated hillsides across the CF are included in the time series analysis. This correlation-based selection leads to

temporal coherence >0.5 east of the CF compared to values of ~0.3 with standard SBAS [*Pepe and Lanari,* 2006]. We correct topographic residuals in the time-domain [*Fattahi and Amelung,* 2013] and perform the final pixel selection based on a temporal coherence threshold of 0.5 to eliminate pixels affected by phase-unwrapping errors. The only ramp removed in our processing is the local oscillator drift correction of the Envisat ASAR instrument [*Marinkovic and Larsen,* 2013]. The remaining signal contains noise contributions from atmospheric delay, modest given the large number of data used, and orbital errors (<1.5 mm/yr/100 km for the hundreds of SAR acquisitions used [*Fattahi and Amelung,* 2014]). Accordingly, we do not perform alignment to an a priori model of deformation based on GPS data, which differs from previous works on interseismic deformation where the long-wavelength signal was contributed from such a model (e.g., Bürgmann et al. [2006]).

We combine ascending and descending velocity maps to retrieve horizontal and vertical displacement fields [*Wright et al.,* 2004]. Given the nearly north-south azimuthal satellite paths and their steep incidence angles, only the east-west component of the horizontal displacement field is resolved. We validate this velocity field by comparing it with data from BAVU3 GPS [*Bürgmann et al.,* 2014], which agree to within 2 mm/yr (Supplementary material Figure 1).

2.2. Characteristically Repeating Earthquakes (CREs) method

To illuminate the 3D geometry of the faults we rely on characteristically repeating earthquakes (CREs). CRE sequences are events occurring in essentially identical locations, with similar magnitudes, and with high waveform correlation coefficients. They are believed to represent small locked asperities that are repeatedly loaded to rupture by surrounding fault creep [*Nadeau and Johnson,* 1998]. The scaling

between recurrence time, seismic moment, and CRE slip, first established at Parkfield [*Nadeau and Johnson,* 1998], is now widely used to obtain fault slip parameters (e.g., Chen et al., [2007]). We evaluate CRE locations using the Double-Difference Real-Time catalog [*Waldhauser and Schaff,* 2008] and cumulative displacement using the empirical relationship between seismic moment and slip [*Nadeau and Johnson*, 1998; *Chen et al.*, 2007] (See Supplementary Material for CRE catalog). The CREs are a subset of the Double-Difference catalog events that precisely illuminate the actively creeping fault plane.

CREs on the HF are described in Shirzaei et al. [2013], CREs on the CF were identified with the following approach. Catalog location, waveform, and phase pick data for events with >M1.2 of the Northern California Seismic System (NCSS) were downloaded from the Northern California Earthquake Data Center (NCEDC). Waveform cross-correlation analysis in the frequency domain using a ~5 second data window starting ~ 0.5 sec before the P-wave phase arrival was performed on pairs of events with hypocentral separations $\leqq$10 km. For event pairs with maximum cross-correlation values >0.6, cross-correlation values are combined with catalog information on magnitude, occurrence time, and location in an initial similarity characterization file (SCF).

A CRE requires at least two events that have nearly identical waveforms, locations, and similar magnitudes [*Nadeau and Johnson,* 1998]. To identify such events we first isolate a master-pair for the sequence by finding a pair in the SCF that satisfies the following criteria: 1) minimum magnitude of both events $\geqq$ M1.75, 2) difference in magnitudes $\leqq$ 0.15, 3) at least 7 channels with maximum cross-correlations >0.6, 4) third quartile (Q3) maximum cross-correlations among channels $\geqq$ 0.95, 5) events separated by at least one year, and 6) routine catalog hypocentral

separations ≦20 km. We then carry out precise double-difference relative relocation and assign an event-pair as a master-pair if their phase-coherency is above 0.92 on 4 or more channels and their relative locations are ≦10 m. The master-pair events waveforms then serve as templates for identification of additional members of the corresponding CRE sequence by forming a similar event group (SEG). An SEG is formed by extracting all events listed in the SCF that have Q3 correlation values above 0.8 with either of the master-events. The waveforms and phase-picks from these events are aligned with the master-event waveform templates to determine the spectral coherence in phase and amplitude and empirical analyses based on a measure of scaled dissimilarity is used to characterize events in a SEG (e.g., Turner et al. [2013]).

3. Results

3.1. Faults' creeping traces

Figure 1a shows the mean horizontal velocity obtained by combining 19 years of SAR data with ascending and descending viewing geometries projected into Hayward-Calaveras parallel motion (N32°W). Both short- (creep, sharp color change across the CF and HF) and long-wavelength (strain accumulation, blue to red color gradient) signals are well resolved given the large amount of SAR data used (>1200 interferograms) and the resulting low contribution of orbital uncertainties. We calculate the InSAR velocity gradient to locate the creeping fault traces (Figure 1b). The gradient map clearly identifies the surface traces of the HF and CF as well as the surface trace of the Silver Creek Fault (SCF) in the Santa Clara Valley. The SCF blocks groundwater flow, resulting in dominantly vertical ground deformation (Supplementary material Figure 2) and a narrow band of horizontal deformation

[*Chaussard et al.,* 2014]. The gradient map shows that creep on the HF continues 15 km farther south than the southernmost alignment array [*McFarland et al.,* 2014] and mapped active trace [*Lienkaemper,* 2008] in the city of Fremont (Figure 1b). This southernmost section of the HF bends southeastward and appears to merge with the CF near 37°21'26"N (black star on Figure 1). The InSAR-derived location of this southern extension of the HF largely agrees with the fault traces identified using high-resolution LiDAR data [*Mynatt et al.,* 2008] (insets Figure 1b). This creep south of Fremont has likely been missed due to its occurrence in vegetated hillsides (brown and green colors in optical image, bottom right inset of Figure 1b) that are prone to landsliding.

To verify that other geodetic datasets allow for this southern extent of creep on the HF we compare the InSAR velocities with 1970-1993 trilateration (EDM) data [*Manaker et al.,* 2003] and post-1993 GPS data from the Bay Area Velocity Unification Model Version 3 (BAVU3) [*d'Alessio et al.,* 2005; *Bürgmann et al.,* 2014] (Figure 2). Profiles at three locations on the HF and CF show a good agreement between InSAR, GPS, and EDM data (Figure 2) despite their different time periods, suggesting relatively steady long-term tectonic deformation. The central profile (dark blue) shows that EDM data allow for creep on the southern HF at 2-5.5 mm/yr as far south as 37°24'35"N. The black profile shows creep accommodated by the CF at rates twice as high as creep on the HF, the creeping traces of these two faults having likely already merged north of 37°20'40"N. These observations support the InSAR gradient map and confirm that the HF and CF surface traces are likely merging near 37°21'26"N. North of this surface junction, aseismic slip is partitioned between the north CF and the HF, while south of it it is accommodated almost entirely by the central CF. Major infrastructure currently crossing this southward extension of the

creeping HF, such as the South Bay Aqueduct, may suffer damage due to creep and earthquake surface ruptures.

3.2. Faults' 3D geometry

To constrain the 3D geometry of the linking fault structure between the HF and CF we rely on CREs, which represent small locked asperities that are repeatedly loaded to rupture by surrounding fault creep. CREs along the CF and HF (Figure 3a) can be grouped in three categories based on their estimated 1992-2011 cumulative slip and their depths: 1) small cumulative slip and intermediate depths (3-7 km), characteristic of the northern HF [*Schmidt et al.,* 2005]; 2) large cumulative slip and intermediate to large depths (3-11 km), characteristic of the central CF; and 3) shallow events (<3 km depth), occurring only at the connection between the HF and CF. The shallow CREs align well with the southernmost section of the creeping HF described above, confirming the connection of the two faults' surface traces at this location. On the other hand, intermediate-depth CREs (>3 km) occur along one continuous fault plane located ~10 km farther north than the surface connection, illuminating the junction at depth between the HF in southern Fremont and the CF (Figure 3). This deep junction is in agreement with previous works [*Andrews et al.*, 1998; *Ponce et al.,* 2004; *Manaker et al.,* 2005; *Williams et al.,* 2005; *Graymer et al.*, 2007; *Hardebeck, et al.,* 2007] and suggests that the HF is transitioning from its near vertical geometry >20 km north of Fremont to splaying off the CF, the deep HF fault plane gradually bending towards the CF with a northeast dip below Mission Peak at depths of ~3-5 km. We develop a model of the 3D geometry of the Hayward-Calaveras junction with surface traces based on the InSAR velocity gradient map and the geometry at depth (dip) derived from the CRE locations (Figure 3b, see Supplementary Material for list of vertices of the 3D mesh). Our new model of the

Hayward-Calaveras Fault zone geometry argues for a direct connection via a dipping wedge-shaped fault plane to reconcile the occurrence of creep 10 km south of the deep Mission Peak connection. Andrews et al. [1998] argue for an additional locked reverse fault or a combination of strike-slip and reverse faults constituting the Mission fault zone, which would accommodate deformation between the HF and CF. Due to the absence of related seismicity and surface deformation, these faults are not included in our model. The dip-slip component associated with the stepover geometry and the observed uplift between the HF and CF could either involve such a secondary shallow reverse fault [*Andrews et al., 1998*] or could occur as oblique slip on the through-going structure of our model.

4. Conclusions

Using space geodetic data we show that the surface creep of the HF continues 15 km farther south than the previously known active trace, revealing new potential for rupture and damage. This strand of the HF, located in vegetated hillsides, bends towards the east and merges with the creeping trace of the CF south of the city of Fremont, arguing for a direct surface connection between the two faults. Using repeating micro-earthquakes we confirm the location of the HF and CF surface junction and show that their direct connection at depth is located ~10 km farther north. A model of the 3D geometry of the faults' structure relying on the InSAR velocity gradient map for surface traces and on CREs for the geometry at depth reveals the 3-D wedge geometry of the connection. Our study illustrates how a combination of space geodesy and seismology can illuminate the structure of active faults.

Our results indicate that the HF and CF should be treated as a single, continuous structure with potential for earthquake ruptures propagating across. The

increased length of a potential rupture involving the Hayward and central Calaveras Faults (up to ~160 km long) could generate earthquakes much larger than M7, especially given that creeping patches may participate in a rupture in the presence of dynamic weakening [*Noda and Lapusta,* 2013]. Our new geometry of the Hayward-Calaveras Fault zone should be used as a basis for earthquake process modeling and ground motion simulations to reevaluate seismic hazard in the Bay Area.

Acknowledgments

We thank the National Aeronautics and Space Administration (NASA) for support through grant NNX12AQ32G and the U.S. Geological Survey National Earthquake Hazards Reduction Program (NEHRP) for support through grants G12AP20096 and G13AP00035. The ERS and Envisat original data are copyrighted by the European Space Agency and were provided through the WInSAR archive. Waveform data, metadata, and data products for this study were accessed through the Northern California Earthquake Data Center [*NCEDC, 2014*]. We thank Jim Lienkaemper and Bob Simpson for their thoughtful comments prior to submission and two anonymous reviewers. Berkeley Seismological Laboratory contribution #15-xxx.

References

Aagaard, B. T., Graves, R. W., Schwartz, D. P., Ponce, D. A. & Graymer, R. W. Ground-Motion Modeling of Hayward Fault Scenario Earthquakes, Part I: Construction of the Suite of Scenarios. *Bulletin of the Seismological Society of America* **100,** 2927–2944 (2010). doi:10.1785/0120090324

Andrews, D.J., Oppenheimer, D.H., and Lienkaemper, J. J. The Mission Link Between the Hayward and Calaveras Faults, *Journal of Geophysical Research*, **98**(B7), 12083–12095 (1993).

Aydin, A., & Page, B. M. Diverse Pliocene-Quaternary Tectonics in a Transform Environment, San-Francisco Bay Region, California. *Geol Soc America Bull* **95,** 1303–1317 (1984).

Berardino, P., Fornaro, G., Lanari, R. & Sansosti, E. A new algorithm for surface deformation monitoring based on small baseline differential SAR interferograms. *IEEE Trans. Geosci. Remote Sensing* **40,** 2375–2383 (2002). doi:10.1109/TGRS.2002.803792

Bürgmann, R., Hilley, G., Ferretti, A., & Novali, F. Resolving vertical tectonics in the San Francisco Bay Area from permanent scatterer InSAR and GPS analysis. *Geology*, **34**(3), 221. doi:10.1130/G22064.1, (2006).

Bürgmann, R., Johanson, I. & Nadeau, R. Time-dependent creep of the Calaveras fault from 18-years of InSAR, GPS and repeating earthquakes. *U.S. Geological Survey, National Earthquake Hazard Reduction Program, Final Technical Report* G13AP00035, 17 p. (2014). http://earthquake.usgs.gov/research/external/reports/G13AP00035.pdf

Chaussard, E., Bürgmann, R., Shirzaei, M., Fielding, E. J. & Baker, B. Predictability of hydraulic head changes and characterization of aquifer- system and fault properties from InSAR- derived ground deformation. *Journal of Geophysical Research-Solid Earth* **119,** 6572–6590 (2014). doi:10.1002/ 2014JB011266.

Chen, C.W. & Zebker, H.A. Two-dimensional phase unwrapping with use of statistical models for cost functions in nonlinear optimization, *Journal of the Optical Society of America A,* **18**(2), 338–351 (2001).

Chen, K. H., Nadeau, R. M. & Rau, R.-J. Towards a universal rule on the recurrence interval scaling of repeating earthquakes? *Geophys. Res. Lett.* **34** (2007). doi:10.1029/2007GL030554

d'Alessio, M. A., Johanson, I. A., Burgmann, R., Schmidt, D. A., & Murray, M. H. Slicing up the San Francisco Bay Area: Block kinematics and fault slip rates from GPS- derived surface velocities. *JGR Solid Earth* **110**(B6). doi:10.1029/2004JB003496, (2005).

Farr, T.G. & Kobrick, M. Shuttle radar topography mission produces a wealth of data, *EOS Trans. AGU*, **81**(48), 583–585 (2000).

Fattahi, H. & Amelung, F. DEM error correction in InSAR time series. *IEEE Trans. Geosci. Remote Sensing* **51,** (2013).

Fattahi, H. & Amelung, F. InSAR uncertainty due to orbital errors. *Geophys J Roy Astr S* **199,** 549–560 (2014). doi:10.1093/gji/ggu276

Field, E. H. *et al.* Long- Term Time- Dependent Probabilities for the Third Uniform California Earthquake Rupture Forecast (UCERF3). *Bulletin of the Seismological Society of America* (2015), doi:10.1785/0120140093

Graymer, R. W., Langenheim, V. E., Simpson, R. W., Jachens, R. C. & Ponce, D. A. Relatively simple through-going fault planes at large-earthquake depth may be concealed by the surface complexity of strike-slip faults. *Geological Society, London, Special Publications* **290,** 189–201 (2007). doi:10.1144/SP290.5

Hardebeck, J. L., Michael, A. J. & Brocher, T. M. Seismic Velocity Structure and Seismotectonics of the Eastern San Francisco Bay Region, California. *Bulletin of the Seismological Society of America* **97,** 826–842 (2007). doi:10.1785/0120060032

Lienkaemper, J. J. Digital database of recently active traces of the Hayward Fault, California. *U.S. Geological Survey Data Series* **177**, version 1.1. (2006, revised 2008) *http://pubs.usgs.gov/ds/2006/177/*

Lienkaemper, J. J., McFarland, F. S., Simpson, R. W. & Caskey, S. J. Using Surface Creep Rate to Infer Fraction Locked for Sections of the San Andreas Fault System in Northern California from Alignment Array and GPS Data. *Bulletin of the Seismological Society of America* (2014). doi:10.1785/0120140117

Lienkaemper, J. J., Williams, P. L. & Guilderson, T. P. Evidence for a Twelfth Large Earthquake on the Southern Hayward Fault in the Past 1900 Years. *Bulletin of the Seismological Society of America* **100,** 2024–2034 (2010). doi:10.1785/0120090129

Lozos, J. C., Oglesby, D. D., Brune, J. N. & Olsen, K. B. Rupture Propagation and Ground Motion of Strike-Slip Stepovers with Intermediate Fault Segments. *Bulletin of the Seismological Society of America* (2014). doi:10.1785/0120140114

Manaker, D. M., Bürgmann, R., Prescott, W. H. & Langbein, J. Distribution of interseismic slip rates and the potential for significant earthquakes on the Calaveras fault, central California. *Journal of Geophysical Research-Solid Earth* **108,** (2003). doi:10.1029/2002JB001749

Manaker, D. M., Michael, A. J. & Bürgmann, R. Subsurface structure and kinematics of the Calaveras-Hayward fault stepover from three-dimensional V-P and seismicity, San Francisco Bay region, California. *Bulletin of the Seismological Society of America* **95,** 446–470 (2005). doi:10.1785/0120020202

Marinkovic, P. & Larsen, Y. Consequences of long-term ASAR local oscillator frequency decay—an empirical study of 10 years of data, *European Space Agency, in Proceedings of the Living Planet Symposium*, Edinburgh, U. K (2013).

McFarland, F. S., Lienkaemper, J. J. & Caskey, S. J. Data from theodolite measurements of creep rates on San Francisco Bay Region faults, California: 1979-2013. *U.S. Geological Survey Open-File Report* 09-1119, **17** (2014).

Mynatt, I., Lienkaemper, J., Whitehill, C., and Prentice, C. Airborne Laser Swath Mapping (ALSM)-based ground mapping of the southern Hayward fault. In Proceedings of the 3rd Conference on earthquake hazards in the eastern San Francisco Bay area: *California Geological Survey Special Report* **219**, 93-99 (2009). https://cloud.sdsc.edu/v1/AUTH_opentopography/www/files/NoCal_GeoES_LiDAR_hs_v3.kmz

Nadeau, R. M. M. & Johnson, L. R. Seismological studies at Parkfield VI: Moment release rates and estimates of source parameters for small repeating earthquakes. *Bulletin of the Seismological Society of America* **88,** 790–814 (1998).

NCEDC (2014), Northern California Earthquake Data Center. UC Berkeley Seismological Laboratory. Dataset. doi:10.7932/NCEDC.

Noda, H. & Lapusta, N. Stable creeping fault segments can become destructive as a result of dynamic weakening. *Nature* **493,** 518–521 (2013). doi:10.1038/nature11703

Oppenheimer, D. H. *et al.* The 2007 M5.4 Alum Rock, California, earthquake: Implications for future earthquakes on the central and southern Calaveras Fault. *Journal of Geophysical Research* **115,** (2010). doi:10.1029/2009JB006683

Pepe, A. & Lanari, R. On the extension of the minimum cost flow algorithm for phase unwrapping of multitemporal differential SAR interferograms, *IEEE Trans. Geosci. Remote Sens.*, **44**(9), 2374–2383 (2006).

Ponce, D. A., Simpson, R. W., Graymer, R. W. & Jachens, R. C. Gravity, magnetic, and high-precision relocated seismicity profiles suggest a connection

between the Hayward and Calaveras Faults, northern California. *Geochem. Geophys. Geosyst.* **5,** (2004). doi:10.1029/2003GC000684

Rosen, P.A., Hensley, S., Joughin, I.R., Li, F., Madsen, S.N., Rodriguez, E. & Goldstein, M. Synthetic aperture radar interferometry, *Proc. IEEE.*, **88**(3), 333–382 (2000).

Schmidt, D. A., Bürgmann, R., Nadeau, R. M. M. & d'Alessio, M. Distribution of aseismic slip rate on the Hayward fault inferred from seismic and geodetic data. *Journal of Geophysical Research-Solid Earth* **110,** (2005). doi:10.1029/2004JB003397

Shirzaei, M. & Bürgmann, R. Time-dependent model of creep on the Hayward fault from joint inversion of 18 years of InSAR and surface creep data. *Journal of Geophysical Research-Solid Earth* **118,** 1733–1746 (2013). doi:10.1002/jgrb.50149

Shirzaei, M., Bürgmann, R. & Taira, T. Implications of recent asperity failures and aseismic creep for time-dependent earthquake hazard on the Hayward fault. *Earth and Planetary Science Letters* **371-372,** 59–66 (2013).

Simpson, G. D., Baldwin, J. N., Kelson, K. I. & Lettis, W. R. Late holocene slip rate and earthquake history for the northern Calaveras fault at Welch Creek, eastern San Francisco Bay area, California. *Bulletin of the Seismological Society of America* **89,** 1250–1263 (1999).

Turner, R. C., Nadeau, R. M. and Bürgmann, R. Aseismic slip and fault interaction from repeating earthquakes in the Loma Prieta aftershock zone, *Geophys. Res. Lett.*, **40**, 1079–1083, doi:10.1002/grl.50212, (2013).

U.S. Geological Survey and California Geological Survey. Quaternary fault and fold database for the United States (accessed Jan 20, 2015), *from USGS web site:* http//earthquake.usgs.gov/hazards/qfaults/

Waldhauser, F. & Schaff, D. P. Large-scale relocation of two decades of Northern California seismicity using cross-correlation and double-difference methods. *Journal of Geophysical Research-Solid Earth* **113,** (2008). doi:10.1029/2007JB005479.

Wesnousky, S. G. Displacement and geometrical characteristics of earthquake surface ruptures: Issues and implications for seismic-hazard analysis and the process of earthquake rupture. *Bulletin of the Seismological Society of America* **98**, 1609-1632 (2008).

Williams, R. A. *et al.* Seismic reflection evidence for a northeast- dipping Hayward fault near Fremont, California: Implications for seismic hazard. *Geophys. Res. Lett.* **32,** (2005). doi:10.1029/2005GL023113

Wright, T. J., Parsons, B. E. & Lu, Z. Toward mapping surface deformation in three dimensions using InSAR. *Geophys. Res. Lett.* **31,** (2004). doi:10.1029/2003GL018827

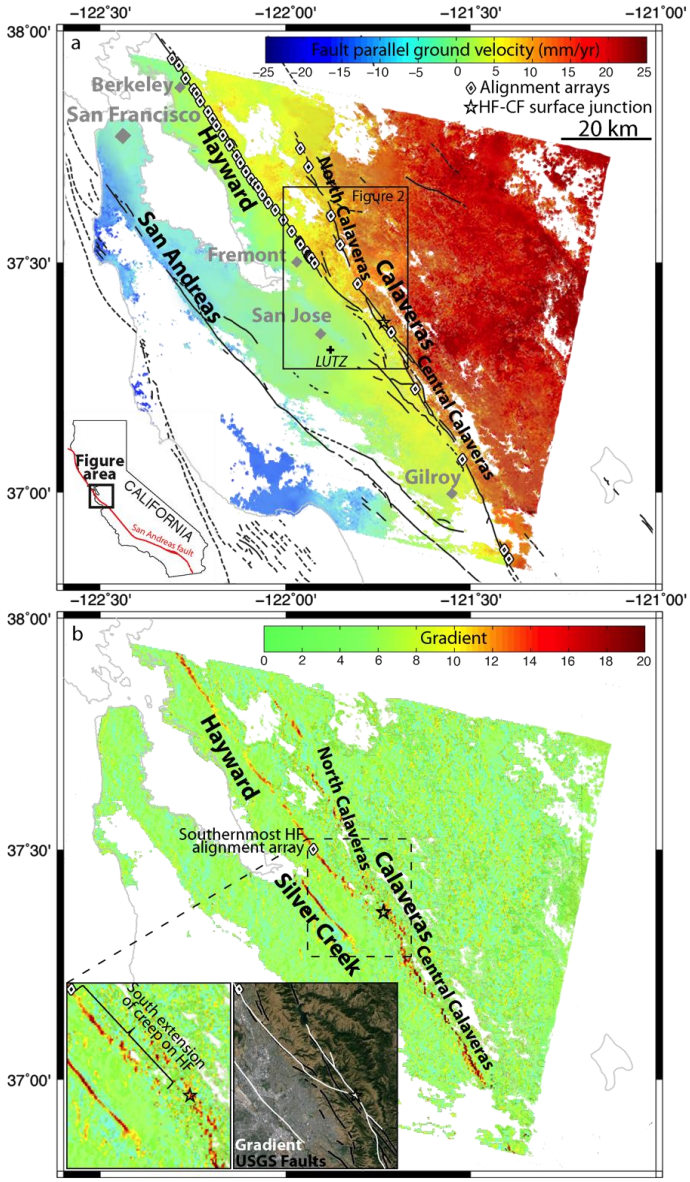

Figure 1: *a) Mean HF-parallel ground velocity from 19 years of InSAR data in the San Francisco Bay Area. Blue colors correspond to northwest motion and red colors to southeast motion with respect to the GPS station LUTZ (cross). The sharp transitions in colors across the Hayward and Calaveras Faults document the interseismic surface creep. Full and dashed black lines indicate mapped fault traces [U.S. Geological Survey and California Geological Survey, 2015] (Hayward and central Calaveras Fault traces being based on LiDAR data [Mynatt et al., 2008]), white diamonds are alignment-array locations, the black star shows the approximate location of the junction between the HF and CF surface traces near 37°21'26"N, and grey diamonds are main cities. The black rectangle shows the location of Figure 2. b) Gradient map derived from the InSAR mean ground velocity. High gradient (red) correspond to the surface traces of creeping faults (HF and CF) and a fault (Silver Creek Fault) blocking groundwater flow in the Santa Clara Valley aquifer [Chaussard et al., 2014]. The dashed rectangle (zoom in the bottom left) highlights the southernmost extension of creep on the HF and the bottom right inset shows the corresponding Landsat optical image with USGS fault traces (black) and fault traces from the gradient map (white).*

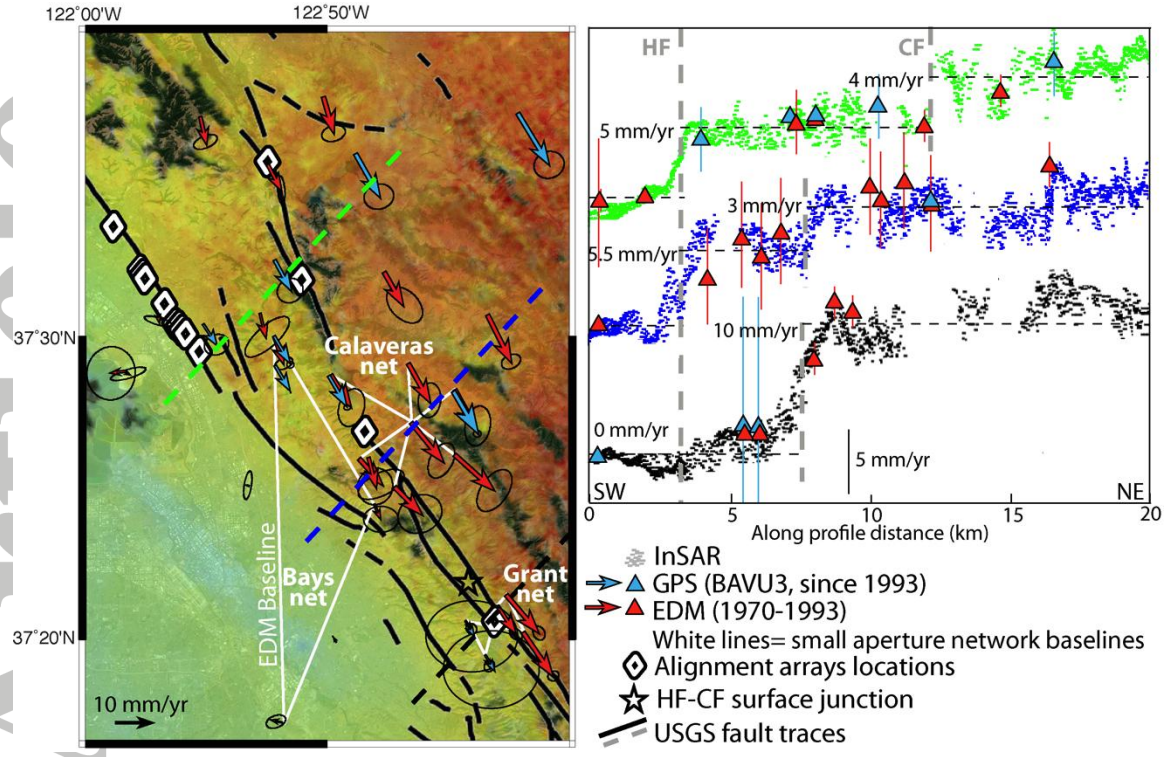

Figure 2: *Left: InSAR mean velocity overlaying optical imagery (same color-scale as Figure 1), velocities from GPS (blue arrows) and EDM (red arrows, baselines of small aperture trilateration networks shown by white lines) near the south HF. The dashed-colored lines indicate the locations of three profiles shown on the right comparing these datasets. Right: profiles at locations with GPS (blue triangles) and EDM (red triangles) data projected to compare with InSAR HF-parallel horizontal velocities. Vertical bars show the data uncertainties, when no bars are visible the uncertainties are <1mm/yr. The dark blue profile confirms that EDM and GPS data allow for continuation of creep at ~5.5 mm/yr on the HF 15 km south of the previously documented termination of active surface creep [Lienkaemper, 2008]. The black profile shows significantly higher creep rates accommodated by the CF suggesting that the two faults have merged north of this location.*

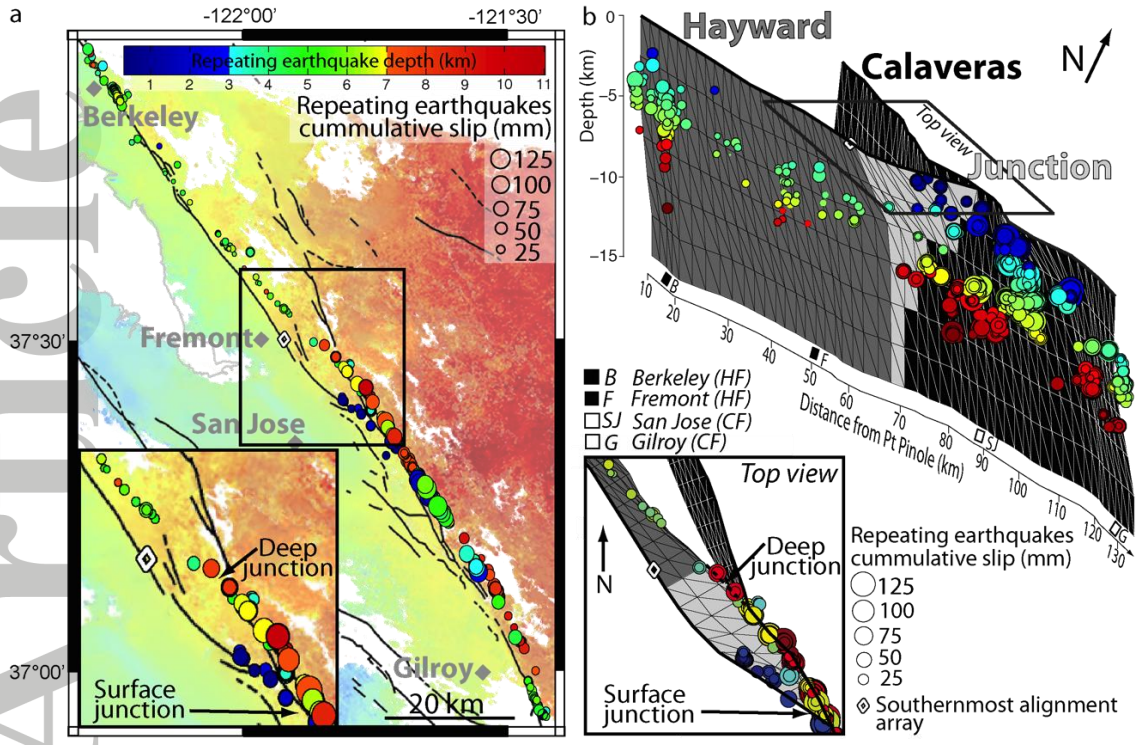

Figure 3: *a) CREs color-coded by depth and with radius proportional to their 1992-2011 cumulative slip overlaying the mean InSAR ground velocity. Shallow CREs (blue) confirm the southward continuation of the HF surface creep and the surface junction with the CF. Continuous CREs between the CF and HF illuminate the junction at depth, 10 km north of the surface junction. The black box (bottom left inset) enlarges the region of the junction. b) Model of the refined geometry of the HF (grey) and CF (black). The surface traces of the faults are based on the InSAR gradient map (Figure 1b) and the geometry at depth is based on the CREs (circles). The light grey mesh highlights the newly established connection between the two faults.*